Supporting Information

Polyoxometalate-Based Metal-Organic Framework on Carbon Cloth with Hot-Pressing Method for High Performance Lithium-Ion Batteries

A-Man Zhang, ‡[a] Mi Zhang, ‡[a] Di Lan,[b] Hai-Ning Wang,[a] Yu-Jia Tang,[a] Xiao-Li Wang,[a] Long-Zhang Dong,[a] Lei Zhang,[a] Shun-Li Li*[a] and Ya-Qian Lan*[a]

[a] Jiangsu Collaborative Innovation Centre of Biomedical Functional Materials, Jiangsu Key Laboratory of New Power Batteries, School of Chemistry and Materials Science, Nanjing Normal University, Nanjing 210023, P. R. China

[b] Faw Jilin Automobile Company, Ltd. (FAWMC), Jilin 132013, P. R. China

E-mail: yqlan@njnu.edu.cn

slli@njnu.edu.cn

‡These authors contribute equally to this work.

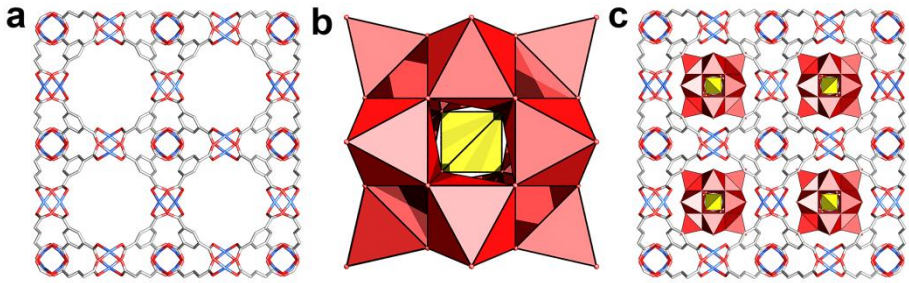

Figure S1. The structures of (a) HKUST-1, (b) PMo_{12} and (c) NENU-5.

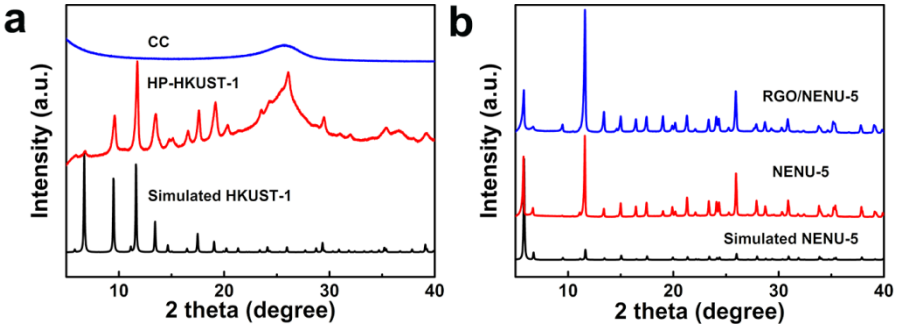

Figure S2. (a) PXRD patterns of carbon cloth (CC), simulated HKUST-1 and HP-HKUST-1/CC. (b) PXRD patterns of simulated NENU-5, NENU-5 and RGO/NENU-5.

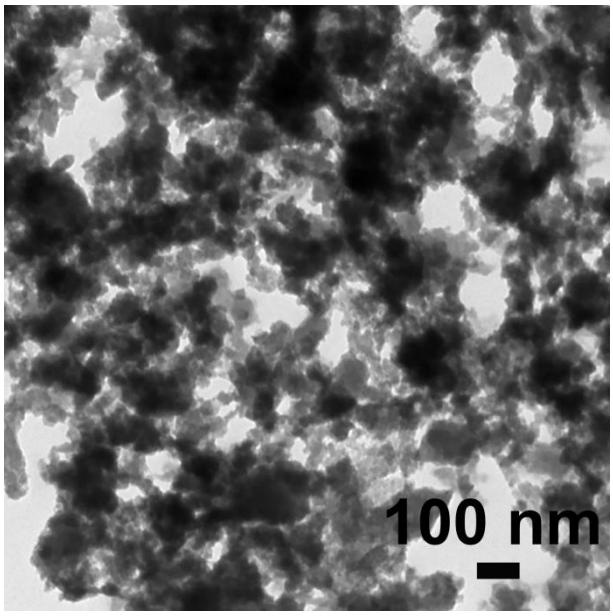

Figure S3. TEM image of HP-NENU-5/CC.

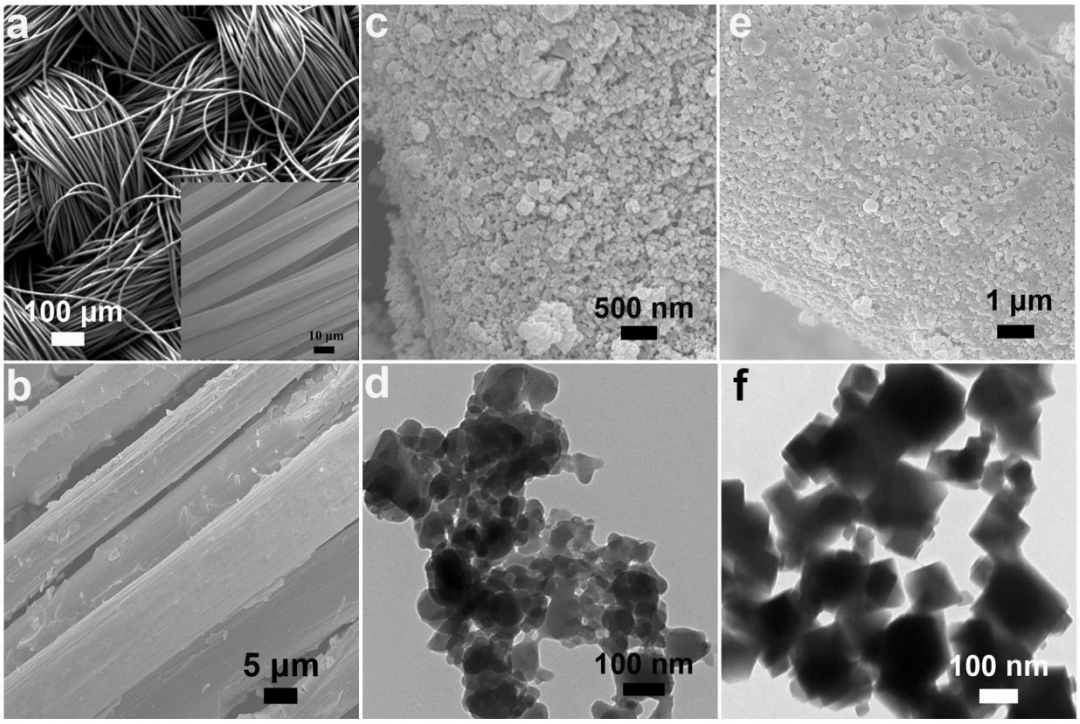

Figure S4. (a) SEM image of bare CC. (b) SEM image of HP-PMo_{12}/CC. (c) SEM image of HP-HKUST-1/CC. (d) TEM image of HP-HKUST-1/CC. (e) SEM image of Pre-NENU-5/CC. (f) TEM image of Pre-NENU-5/CC.

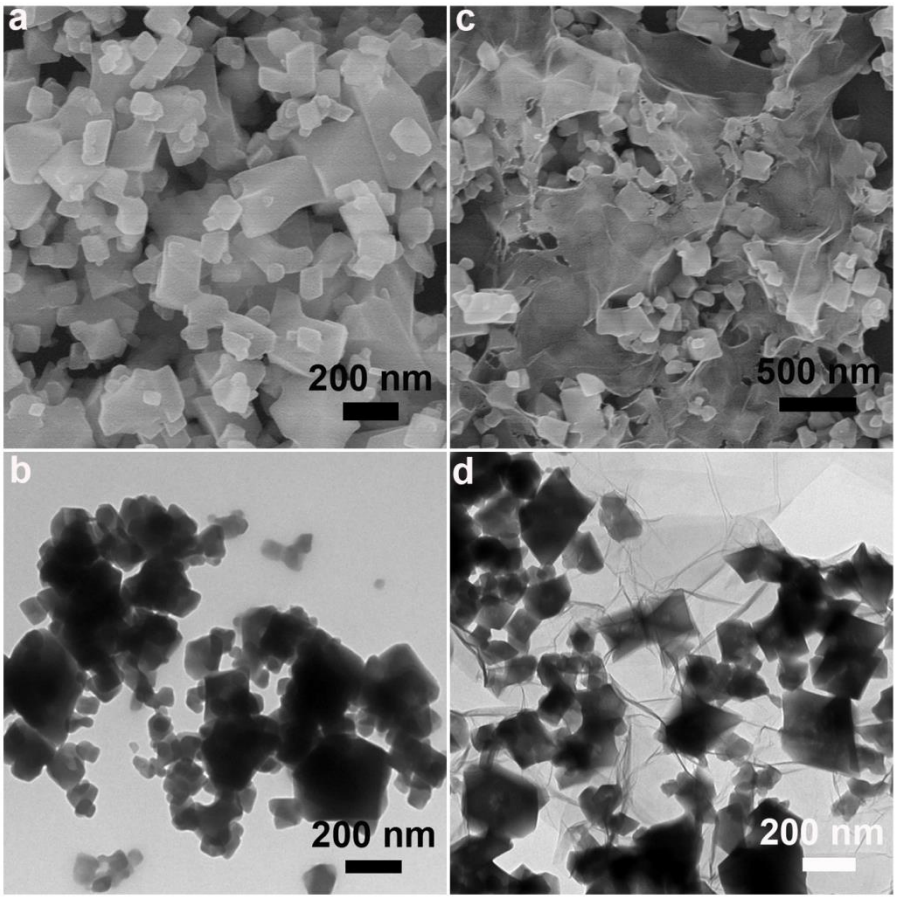

Figure S5. (a) SEM image of NENU-5. (b) TEM image of NENU-5. (c) SEM image of RGO/NENU-5. (d) TEM image of RGO/NENU-5.

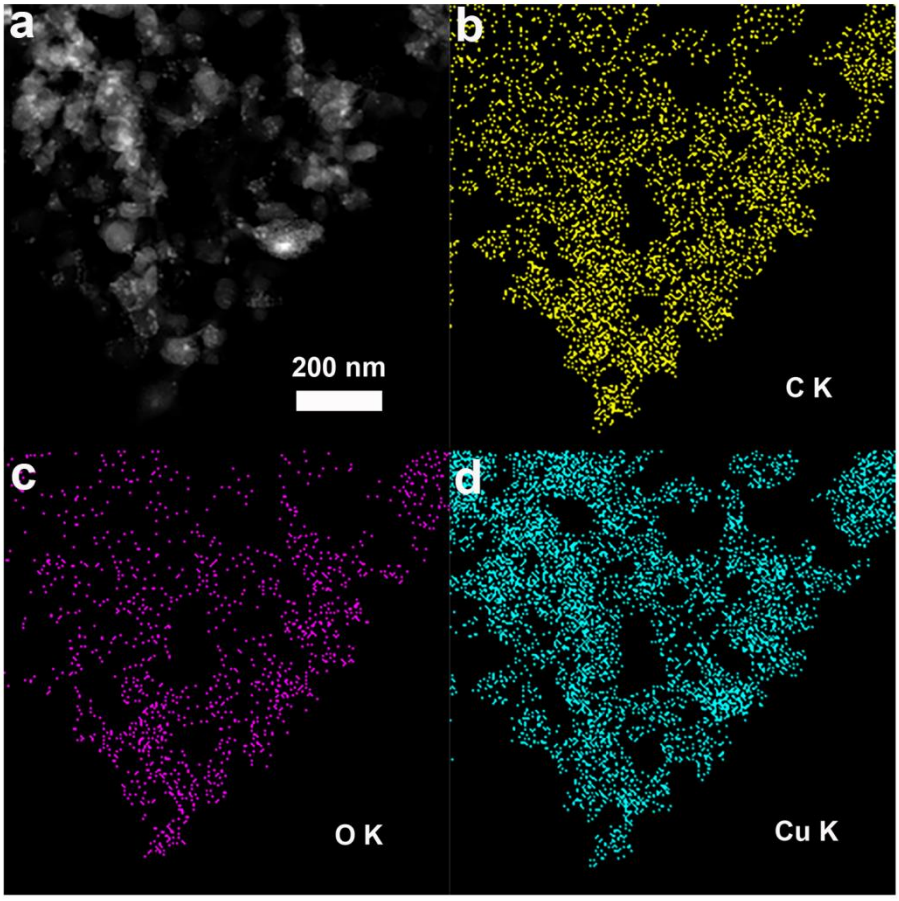

Figure S6. (a) STEM image of HP-HKUST-1/CC and the corresponding mapping images of (b) C, (c) O and (d) Cu.

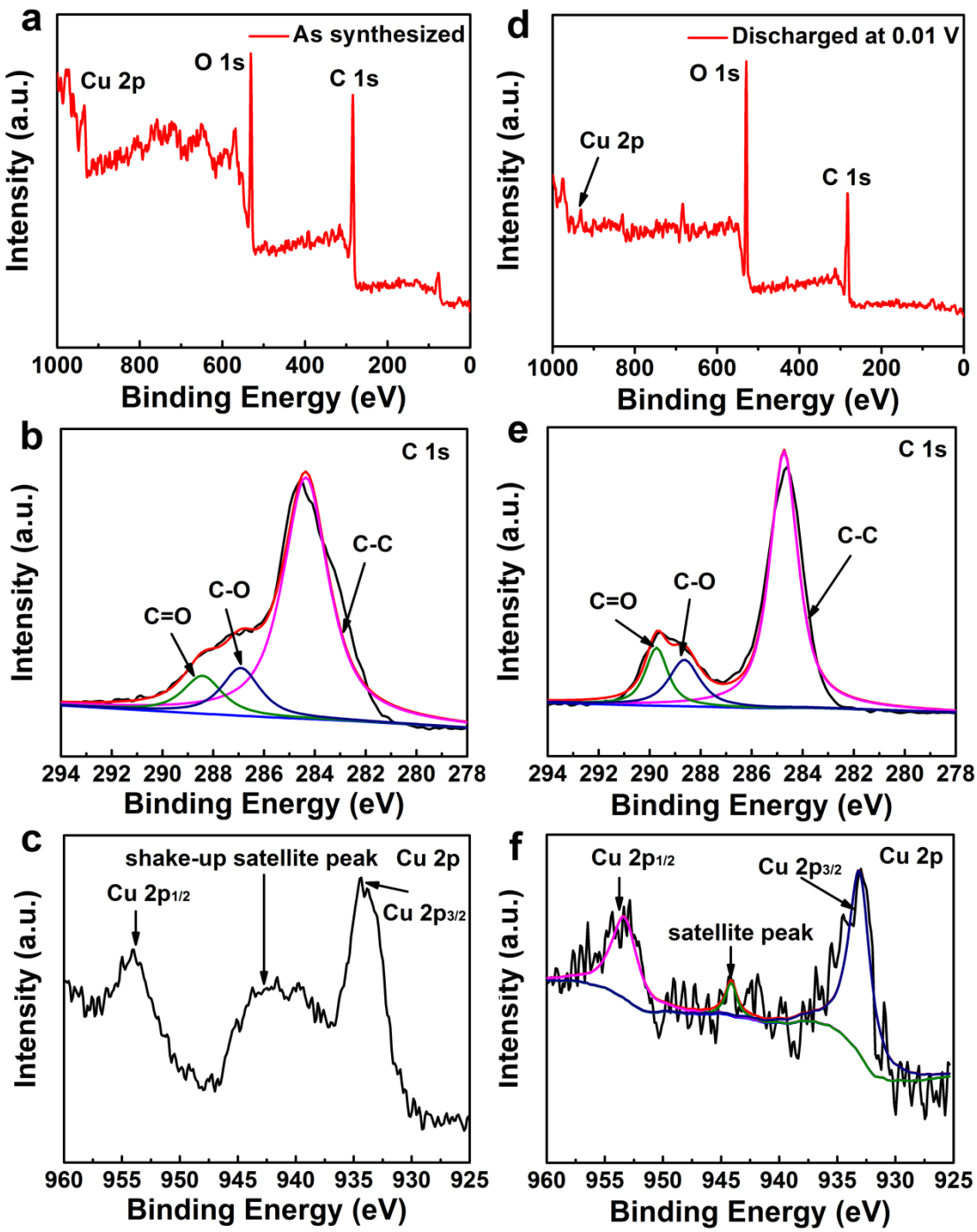

Figure S7. XPS spectra of HP-HKUST-1/CC before and after discharged at 0.01 V. (a-c): As synthesized sample, (a) survey scan. (b) C 1s. (c) Cu 2p; (d-f): Discharged at 0.01 V, (d) survey scan. (e) C 1s. (f) Cu 2p.

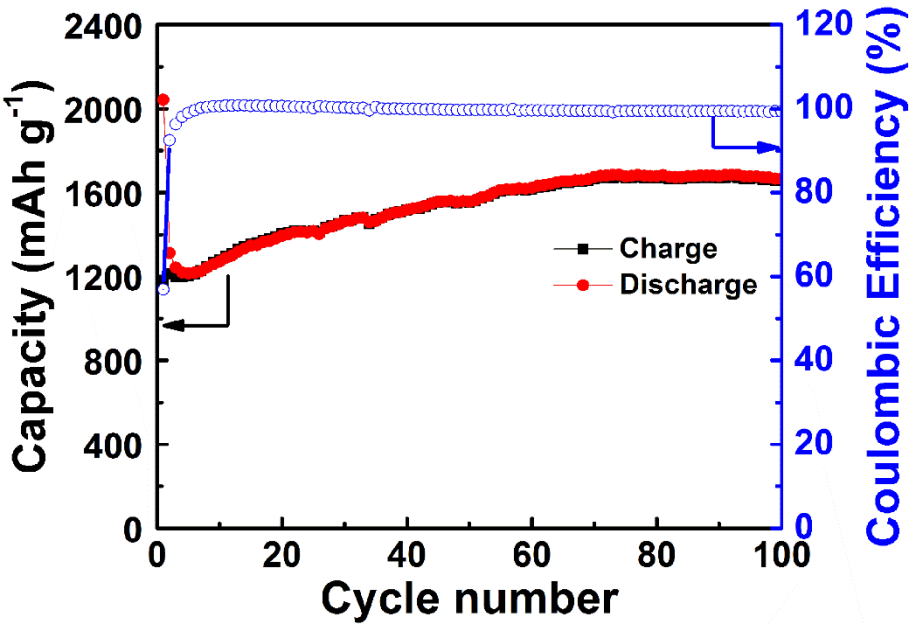

Figure S8. Cycling performance of Pre-NENU-5/CC at a current density of 200 mA g^{-1}.

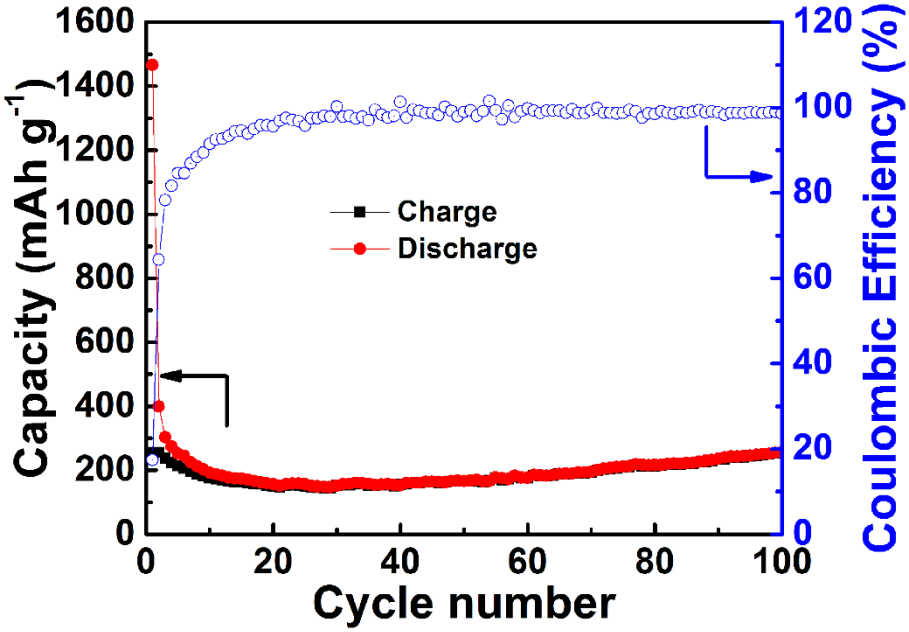

Figure S9. Cycling performance of NENU-5 (the current collector is copper foil) at a current density of 50 mA g^{-1}.

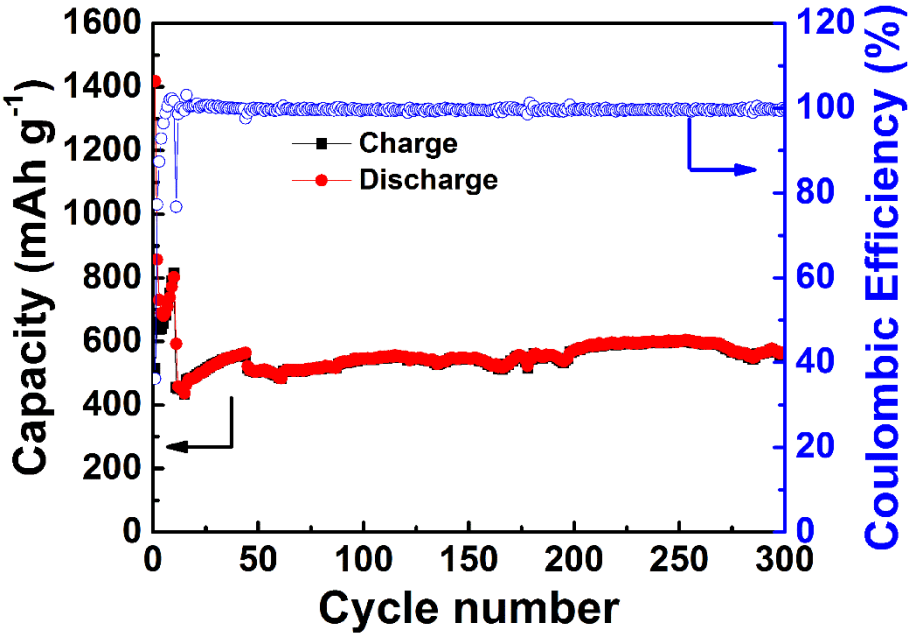

Figure S10. Cycling performance of RGO/NENU-5 (the current collector is copper foil) at a current density of 1000 mA g^{-1}.

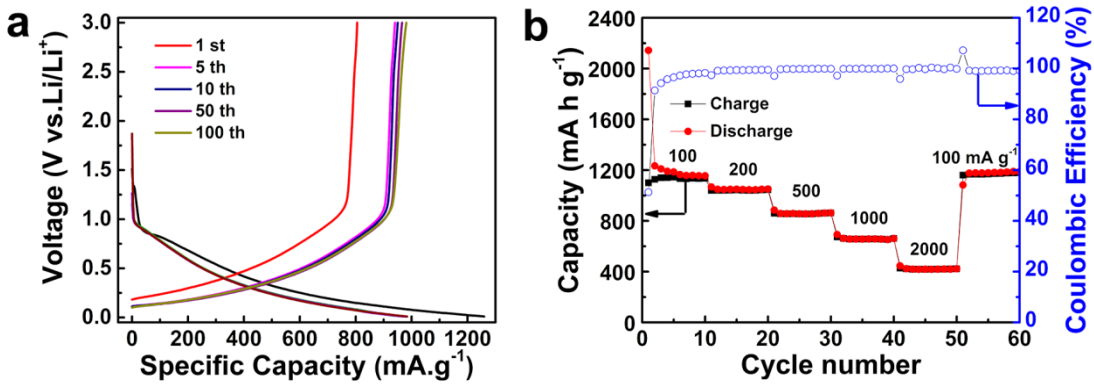

Figure S11. (a) Charge/discharge profiles of HP-HKUST-1/CC for different cycles constantly at 200 mA g^{-1}. (b) HP-HKUST-1/CC cycled at various current densities from 100 mA g^{-1} to 2000 mA g^{-1}.

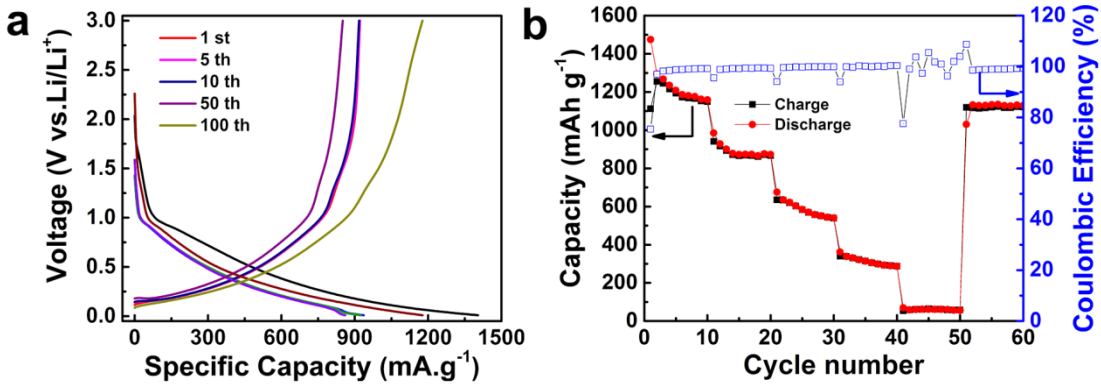

Figure S12. (a) Charge/discharge profiles of HP-PMo_{12}/CC for different cycles constantly at 200 mA g^{-1}. (b) HP- PMo_{12}/CC cycled at various current densities from 100 mA g^{-1} to 2000 mA g^{-1}.

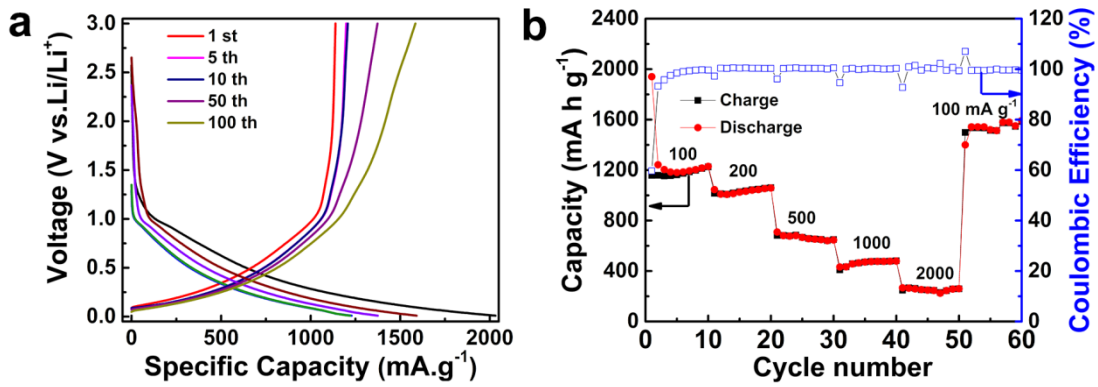

Figure S13. (a) Charge/discharge profiles of Pre-NENU-5/CC for different cycles constantly at 200 mA g^{-1}. (b) Pre-NENU-5/CC cycled at various current densities from 100 mA g^{-1} to 2000 mA g^{-1}.

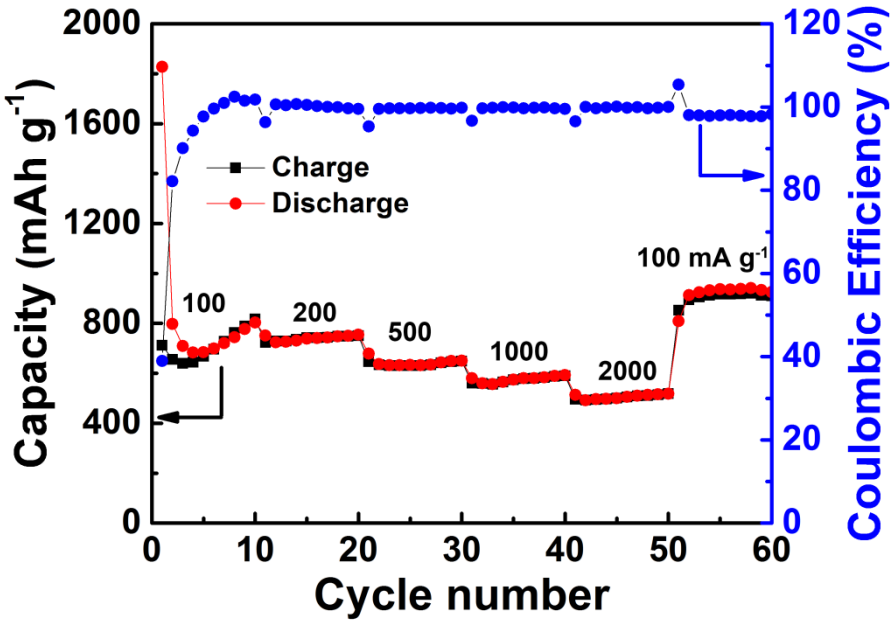

Figure S14. RGO/NENU-5 cycled at various current densities from 100 mA g^{-1} to 2000 mA g^{-1}.

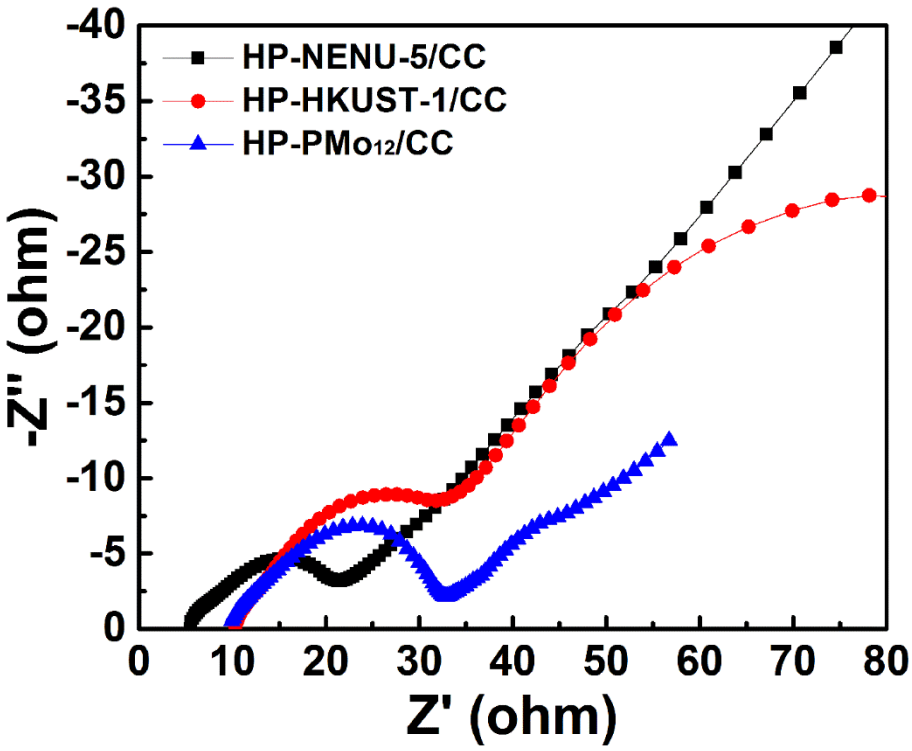

Figure S15. Nyquist plots of the HP-NENU-5/CC, HP-HKUST-1/CC and HP-PMo_{12}/CC after charging and discharging.

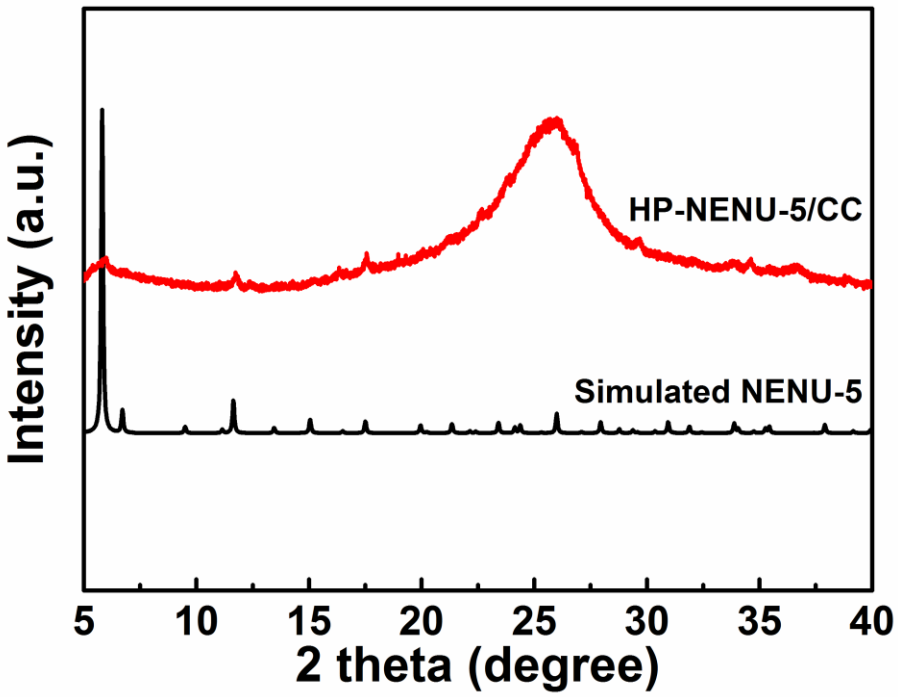

Figure S16. PXRD patterns of simulated NENU-5 and the HP-NENU-5/CC after charging and discharging.

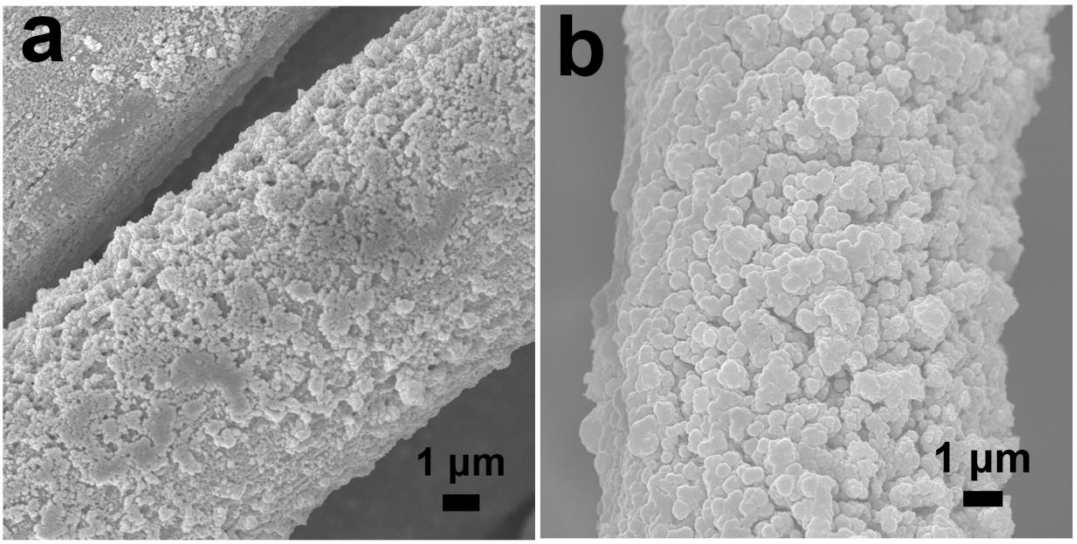

Figure S17. (a) SEM of the HP-NENU-5/CC. (b) SEM of the HP-NENU-5/CC after charging and discharging at the current density of 500 mA g^{-1} for 100 cycles.

Table S1. Comparison of HP-NENU-5/CC with other pristine MOFs, POMs (not used as a template, such as carbonation) and CC-based anodes.

Materials	CD (mA g^{-1})	Cycles / RC (mAh g^{-1})	Biggest CD (mA g^{-1}) / cycles	AMR (%)	Ref.
HP-NENU-5/CC	**200 (or 130 mA cm^{-2})**	**100 / 1723**	**1000 (or 650 mA cm^{-2}) / 400**	**1.8-2.2 mg cm^{-2}**	**This work**
POM-based anodes					
POM/CNT	0.5 mA cm^{-2}	100 / 850	1 mA cm^{-2} / 10	80	[1]
$[MnMo_6O_{24}]^{9-}$/SWNTs	0.5 mA cm^{-2}	100 / 932	1 mA cm^{-2} / 10	50	[2]
Pyrene-Anderson-CNTs	0.5 mA cm^{-2}	100 / 665	1 mA cm^{-2} / 10	30	[3]
Mo_6O_{18}-SCN	50	100 / 876	-	40	[4]
SiW_{11}– CNTs	0.5 mA cm^{-2}	100 / 650	1 mA cm^{-2} / 10	30	[5]
SWNTs/Py–SiW_{11}	0.5 mA cm^{-2}	100 / 580	1 mA cm^{-2} / 10	30	[6]
NAM-EDAG	100	100/above 1000	5000/more than 1000	80	[7]
GO-IL-P_2Mo_{18}	100	100/973	100/1000	80	[8]
$PMo_{10}V_2$/PDA	100	100/915.3	1000/300	70	[9]
MOF-based anodes					
Li/Ni-NTC	100	80 / 482	-	60	[10]
Mn−LCP	50	50 / 390	-	80	[11]
$Zn_3(HCOO)_6$	60	60 / 560	1560 / 20	70	[12]

Co-BTC-CPs	100	100 / 879	2000 / 500	70	[13]
Fe_2O_3@UTSA-74	200	45 / 650	-	70	[14]
$Co_2(OH)_2$(bdc)	50	100 / 650	500 / 10	70	[15]
Mn-BTC	103	100 / 694	2061 / 10	70	[16]
$Zn(IM)_{1.5}(abIM)_{0.5}$	100	200 / 190	400 / 200	70	[17]
Cu-BTC	96	100 / 740	383/ 50	70	[18]
Asp-Cu	50	200 / 233	400 / 100	70	[19]
MIL-53(Fe)@RGO	100	100/550	-	70	[20]
NENU-601	100	200/780	500/200		[21]
POMOF-based anodes					
POMOF-1	1.25 C	500 / 350	-	65	[22]
PMG-3	50	100/1075	3000/400	70	[23]
NENU-507	100	100/640	-	50	[24]
NUU-11	50	200/750	500/400	70	[25]
Compound 1	100	100/570	-	70	[26]
CC-based anodes					
ZnO@ZnO QDs/C	500	100/699	-	1.7-2 mg cm^{-2}	[27]
Cu/CC	210	40/1233	-	-	[28]
MoS_2@CC	100	100/1125	2000/500	-	[29]
Co_3O_4/CC@Gr	100	300/391	-	-	[30]

RC: Reversible capacity. CD: Current density. AMR: Active material ratio.

Reference

(1) Hu, J.; Ji, Y.; Chen, W.; Streb, C.; Song, Y.-F. "Wiring" redox-active polyoxometalates to carbon nanotubes using a sonication-driven periodic functionalization strategy. *Energy Environ. Sci.* **2016,** *9*, 1095-1101.

(2) Ji, Y.; Hu, J.; Huang, L.; Chen, W.; Streb, C.; Song, Y.-F. Covalent attachment of anderson-type polyoxometalates to single-walled carbon nanotubes gives enhanced performance electrodes for lithium ion batteries. *Chem. - Eur. J.* **2015,** *21*, 6469-6474.

(3) Huang, L.; Hu, J.; Ji, Y.; Streb, C.; Song, Y.-F. Pyrene-anderson-modified CNTs as anode materials for lithium-ion batteries. *Chem. - Eur. J.* **2015,** *21*, 18799-18804.

(4) Ramesh, P.; Shalini, B.; Fadnavis, N. W. Knoevenagel condensation of diethylmalonate with aldehydes catalyzed by immobilized bovine serum albumin (BSA). *RSC Adv* **2014,** *4*, 7368-7373.

(5) Chen, W.; Huang, L.; Hu, J.; Li, T.; Jia, F.; Song, Y.-F. Connecting carbon nanotubes to polyoxometalate clusters for engineering high-performance anode materials. *Phys. Chem. Chem. Phys.* **2014,** *16*, 19668-19673.

(6) Ma, D.; Liang, L.; Chen, W.; Liu, H.; Song, Y.-F. Covalently tethered polyoxometalate–pyrene hybrids for noncovalent sidewall functionalization of single-walled carbon nanotubes as high-performance anode material. *Adv. Funct. Mater.* **2013,** *23*, 6100-6105.

(7) Xie, J.; Zhang, Y.; Han, Y.; Li, C. High-capacity molecular scale conversion anode enabled by hybridizing cluster-type framework of high loading with amino-functionalized graphene. *ACS Nano* **2016,** *10*, 5304-5313.

(8) Hu, J.; Diao, H.; Luo, W.; Song, Y.-F. Dawson-type polyoxomolybdate anions ($P_2Mo_{18}O_6^{26-}$) captured by ionic liquid on graphene oxide as high-capacity anode material for lithium-ion batteries. *Chem. - Eur. J.* **2017,** *23*, 8729-8735.
(9) Ding, Y.-H.; Peng, J.; Khan, S.-U.; Yuan, Y. A New Polyoxometalate (POM)-Based Composite: Fabrication through POM-Assisted Polymerization of Dopamine and Properties as Anode Materials for High-Performance Lithium-Ion Batteries. *Chem. - Eur. J.* **2017,** *23*, 10338-10343.
(10) Han, X.; Yi, F.; Sun, T.; Sun, J. Synthesis and electrochemical performance of Li and Ni 1,4,5,8-naphthalenetetracarboxylates as anodes for Li-ion batteries. *Electrochem. Commun.* **2012,** *25*, 136-139.
(11) Liu, Q.; Yu, L.; Wang, Y.; Ji, Y.; Horvat, J.; Cheng, M.-L.; Jia, X.; Wang, G. Manganese-based layered coordination polymer: Synthesis, structural characterization, magnetic property, and electrochemical performance in lithium-ion batteries. *Inorg. Chem.* **2013,** *52*, 2817-2822.
(12) Saravanan, K.; Nagarathinam, M.; Balaya, P.; Vittal, J. J. Lithium storage in a metal organic framework with diamondoid topology - a case study on metal formates. *J. Mater. Chem.* **2010,** *20*, 8329-8335.
(13) Li, C.; Lou, X.; Shen, M.; Hu, X.; Guo, Z.; Wang, Y.; Hu, B.; Chen, Q. High anodic performance of Co 1,3,5-benzenetricarboxylate coordination polymers for Li-ion battery. *ACS Appl. Mater. Interfaces* **2016,** *8*, 15352-15360.
(14) Yan, C. S.; Gao, H. Y.; Le Gong, L.; Ma, L. F.; Dang, L. L.; Zhang, L.; Meng, P. P.; Luo, F. MOF surface method for the ultrafast and one-step generation of metal-oxide-NP@MOF composites as lithium storage materials. *J. Mater. Chem. A* **2016,** *4*, 13603-13610.
(15) Gou, L.; Hao, L.-M.; Shi, Y. X.; Ma, S.-L.; Fan, X.-Y.; Xu, L.; Li, D.-L.; Wang, K. One-pot synthesis of a metal-organic framework as an anode for Li-ion batteries with improved capacity and cycling stability. *J. Solid State Chem.* **2014,** *210*, 121-124.
(16) Maiti, S.; Pramanik, A.; Manju, U.; Mahanty, S. Reversible lithium storage in manganese 1,3,5-Benzenetricarboxylate metal-organic framework with high capacity and rate performance. *ACS Appl. Mater. Interfaces* **2015,** *7*, 16357-16363.
(17) Lin, Y.; Zhang, Q.; Zhao, C.; Li, H.; Kong, C.; Shen, C.; Chen, L. An exceptionally stable functionalized metal-organic framework for lithium storage. *Chem. Commun.* **2015,** *51*, 697-699.
(18) Maiti, S.; Pramanik, A.; Manju, U.; Mahanty, S. Cu_3(1,3,5-benzenetricarboxylate)$_2$ metal-organic framework: A promising anode material for lithium-ion battery. *Microporous Mesoporous Mater* **2016,** *226*, 353-359.
(19) Zhao, C.; Shen, C.; Han, W. Metal-organic nanofibers as anodes for lithium-ion batteries. *RSC Adv* 2015**,** 5, 20386-20389.
(20) Zhang, C.; Hu, W.; Jiang, H.; Chang, J.-K.; Zheng, M.; Wu, Q.-H.; Dong, Q. Electrochemical performance of MIL-53(Fe)@RGO as an Organic Anode Material for Li-ion Batteries. *Electrochim. Acta* **2017,** *246*, 528-535.
(21) Li, X.-X.; Shen, F.-C.; Liu, J.; Li, S.-L.; Dong, L.-Z.; Fu, Q.; Su, Z.-M.; Lan, Y.-Q. A highly stable polyoxometalate-based metal-organic framework with an ABW zeolite-like structure. *Chem. Commun.* **2017,** *53*, 10054-10057.
(22) Yue, Y.; Li, Y.; Bi, Z.; Veith, G. M.; Bridges, C. A.; Guo, B.; Chen, J.; Mullins, D. R.; Surwade, S. P.; Mahurin, S. M.; Liu, H.; Paranthaman, M. P.; Dai, S. A POM-organic framework anode for Li-ion battery. *J. Mater. Chem. A* **2015,** *3*, 22989-22995.

(23) Wei, T.; Zhang, M.; Wu, P.; Tang, Y.-J.; Li, S.-L.; Shen, F.-C.; Wang, X.-L.; Zhou, X.-P.; Lan, Y.-Q. POM-based metal-organic framework/reduced graphene oxide nanocomposites with hybrid behavior of battery-supercapacitor for superior lithium storage. *Nano Energy* **2017,** *34*, 205-214.
(24) Wang, Y.-Y.; Zhang, M.; Li, S.-L.; Zhang, S.-R.; Xie, W.; Qin, J.-S.; Su, Z.-M.; Lan, Y.-Q. Diamondoid-structured polymolybdate-based metal-organic frameworks as high-capacity anodes for lithium-ion batteries. *Chem. Commun.* **2017,** *53*, 5204-5207.
(25) Huang, Q.; Wei, T.; Zhang, M.; Dong, L.-Z.; Zhang, A. M.; Li, S.-L.; Liu, W.-J.; Liu, J.; Lan, Y.-Q. A highly stable polyoxometalate-based metal-organic framework with π-π stacking for enhancing lithium ion battery performance. *J. Mater. Chem. A* **2017,** *5*, 8477-8483.
(26) Yang, X.-Y.; Wei, T.; Li, J.-S.; Sheng, N.; Zhu, P.-P.; Sha, J.-Q.; Wang, T.; Lan, Y.-Q. Polyoxometalate-incorporated metallapillararene/metallacalixarene metal-organic frameworks as anode materials for lithium ion batteries. *Inorg. Chem.* **2017,** *56*, 8311-8318.
(27) Zhang, G.; Hou, S.; Zhang, H.; Zeng, W.; Yan, F.; Li, C. C.; Duan, H. High-performance and ultra-stable lithium-ion batteries based on MOF-derived ZnO@ZnO quantum dots/C core-shell nanorod arrays on a carbon cloth anode. *Adv. Mater.* **2015,** *27*, 2400-2405.
(28) Bai, B.; Liu, Q. Enhanced cycle performance of silicon-based anode by annealing Cu-coated carbon cloth current collector for flexible lithium-ion battery. *Catal. Lett.* **2017,** *147*, 2962-2966.
(29) Wang, T.; Sun, C.; Yang, M.; Zhao, G.; Wang, S.; Ma, F.; Zhang, L.; Shao, Y.; Wu, Y.; Huang, B.; Hao, X. Phase-transformation engineering in MoS_2 on carbon cloth as flexible binder-free anode for enhancing lithium storage. *J. Alloys Compd.* **2017,** *716*, 112-118.
(30) Xie, Q.; Zhang, Y.; Zhu, Y.; Fu, W.; Zhang, X.; Zhao, P.; Wu, S. Graphene enhanced anchoring of nanosized Co_3O_4 particles on carbon fiber cloth as free-standing anode for lithium-ion batteries with superior cycling stability. *Electrochim. Acta* **2017**, *247*, 125-131.